Int. J. Electrochem. Sci., 14 **(2019)** 75 – 90, doi: 10.20964/2019.01.52

International Journal of
ELECTROCHEMICAL
SCIENCE
www.electrochemsci.org

Corrosion Inhibition Effect of Molybdate on Fine-Grain High-Strength Reinforcement in Simulated Concrete Pore Solutions Containing Cl^-

Bilan Lin[1,2,*] *and Yuye Xu*[3]

[1] School of Material Science and Engineering, Xiamen University of Technology, Xiamen 361024, China
[2] Key Laboratory of Functional Materials and Applications of Fujian Province, Xiamen 361024, China
[3] College of Civil Engineering, Huaqiao University, Xiamen, Fujian 361021, China
[*]E-mail: linbilan@xmut.edu.cn

Received: 10 October 2018 / *Accepted:* 31 October 2018 / *Published:* 30 November 2018

To improve the corrosion resistance of fine-grain high-strength (FGHS) reinforcement, molybdate was investigated as a inhibitor. The influence of molybdate on the corrosion behavior of FGHS reinforcement in simulated concrete pore (SCP) solutions containing 1.0% or 3.5% NaCl was evaluated using polarization, electrochemical impedance spectroscopy, and Mott–Schottky curves. The corrosion products were analyzed using scanning electron microscopy and energy-dispersive X-ray spectroscopy. The results revealed that upon increasing the molybdate content, the corrosion current density (i_{corr}) and donor density initially rapidly decreased and then slightly increased, while the corrosion protection efficiency and impedance first rapidly increased and then slightly decreased. The optimum molybdate was 1.0 g/L. The i_{corr} of the former (0.058 μA cm^{-2}) was considerably less than that of the latter (0.250 μA cm^{-2}). The Mott–Schottky curves for the former were continuous, whereas some of those for the latter were discontinuous owing to the depletion of a less Fe^{3+} in the corrosion product. Almost no pits on the reinforcement were observed for the former, whereas a few pits were still observed for the latter. Molybdate exhibited good corrosion inhibition of FGHS reinforcement at low chloride concentrations, although other or composite inhibitors should be considered for high chloride concentrations.

Keywords: Reinforcement; Fine grain; Corrosion; Inhibitor; Molybdate

1. INTRODUCTION

Fine-grain high-strength (FGHS) reinforcement is a new type of steel material in China, in which the main strengthening mechanisms are the formation of fine grains and precipitation, and it is

produced using an optimal combination of microalloying and the thermo-mechanical control process. FGHS reinforcement is mainly used as a structural steel for engineering applications and has become a leading reinforcement material worldwide [1–3]. It is also known as "low-alloy high-strength structural steel" and "thermo-mechanically treated (TMT) steel bar", and has been referred to as "a new generation of steel materials" [4–6]. Fine grains improve the mechanical properties such as strength, toughness, plasticity, etc. However, the presence of more grain boundaries increases the electrochemical heterogeneity in corrosive media, leading to greater corrosion and damage. Recent studies of FGHS reinforcement have mainly focused on the mechanical properties of these materials, their bonding properties with concrete, and the bearing capacity of reinforced concrete structures [7–9], whereas research into corrosion and corrosion protection remains limited [10, 11].

The existing literature shows that the corrosion resistance of fine-grain reinforcement is generally inferior to that of ordinary carbon steel (i.e., plain reinforcement). Shi et al. reported that the stability and corrosion resistance of fine-grain steel in simulated alkaline concrete solutions without chloride ions were slightly superior to those of ordinary carbon steel, but the pitting of the former was more severe than that of the latter in the presence of chloride ions [12, 13]. The main reasons for this were the presence of more grain boundaries and more inclusions in the grain boundaries. The passivation performance of TMT steel was also reported to be superior to that of carbon steel in pure simulated concrete pore (SCP) medium [14]. However, when they were galvanically coupled and the SCP medium contained chloride ions, the TMT steel acted as an anode and the corrosion activity increased. In previous studies [15], the sensitivity of FGHS reinforcement to corrosion by chloride ions and carbonation was found to be greater than that of carbon steel. Corrosion inhibition by nitrate, phosphate, or dioctyl sebacate was also reported to be more inferior for the former than for the latter [16-18]. Similarly, phytic acid and benzotriazole, which are effective corrosion inhibitors for carbon steel, do not inhibit the corrosion of FGHS reinforcement [19].

Moreover, previous studies suggest that improving the strength of the reinforcement is likely to result in reduced corrosion resistance [20-26]. Mohammed et al. [20, 21] found that deformed reinforcement, i.e., low-alloy steel with higher strength, is more vulnerable to corrosion than plain reinforcement. Jiang et al. [23] compared the corrosion behavior of plain and deformed reinforcements in concrete-containing chloride ions, and also observed a greater corrosion rate for deformed reinforcement than plain reinforcement. Geng et al. [24] reported that the corrosion resistance of deformed reinforcement with a yield strength grade of 335 MPa was clearly inferior to that of plain reinforcement. Gan et al. [25] investigated the corrosion behavior of macrocells with various connections, and suggested that the same reinforcement or insulated connections should be used in the reinforcement skeleton. The influence of the substitution ratio of fly ash on the corrosion behavior of deformed reinforcement was reported to be similar to that of plain reinforcement, but the former was found to exhibit a higher corrosion rate than the latter in most cases [26]. In contrast, Islam [11] found that the strength of the reinforcement had no effect on the corrosion resistance. Furthermore, Wang et al. [27] reported that the corrosion of plain reinforcement resulted in greater deterioration of the bending properties of reinforced concrete beams than the corrosion of deformed reinforcement. Therefore, to ensure the safety and durability of concrete structures, further investigation of the corrosion behavior of FGHS reinforcement is crucial.

Corrosion inhibitors are an economical and effective means of protecting reinforcement against corrosion and have been widely applied in reinforced concrete structures. Molybdate is commonly used to inhibit the corrosion of metals [28-30]. Refaey et al. [31] found that increasing the molybdate content of low-carbon steel causes a positive shift in its pitting potential in chloride solution and the adsorption of molybdate on steel surfaces plays an important role in corrosion inhibition. Zheng et al. [32] reported that the physical adsorption of molybdate on duplex stainless steel inhibits pitting and hydrogen permeation. Zhou et al. [33] demonstrated that the pitting of carbon steel was inhibited in $NaCl+NaHCO_3$ solution with molybdate inhibitor, owing to the adsorption of molybdate, the formation of iron molybdate, and the oxidation of Fe^{2+} to Fe_2O_3. Although molybdate is a weaker inhibitor of the pitting corrosion of low-carbon steel in chloride solution than nitrite, it promotes repassivation of the pits far better [34]. Recently, molybdate was also used to inhibit the corrosion of concrete reinforcement [35-37]. At low concentrations, molybdate was found to be a superior corrosion inhibitor than nitrate for reinforcement in SCP solution contaminated by acid rain, although at high concentrations their inhibitory effects were similar [37]. The corrosion inhibitors 1,3-thiazolidin-2-one, benzotriazole, cerium nitrate, and sodium molybdate were compared for reinforcement in SCP solution [38], and only the environmentally friendly molybdate inhibited both the pitting corrosion and uniform corrosion and prolonged the service life of the reinforcement. Here, the inhibition mechanism by molybdate was similar to that previously reported [33]. Zhou et al. [39] also reported that molybdate is a good corrosion inhibitor for reinforcement and increases the carrier density, compactness, and stability of the passivation film.

In this study, the inhibition of the corrosion of FGHS reinforcement in SCP solutions containing 1.0% or 3.5% NaCl by sodium molybdate was investigated using potentiodynamic polarization, electrochemical impedance spectroscopy (EIS), and Mott–Schottky curves. The microscopic structures of the corrosion products were analyzed by scanning electron microscopy (SEM) and energy-dispersive X-ray spectroscopy (EDS). The corrosion inhibition mechanism is also discussed.

2. EXPERIMENTAL

2.1 Materials and reagents

The tested FGHS reinforcements were provided by Fujian Sansteel Group Limited Liability Company. The diameter was 16 mm. The chemical composition (mass fraction) was as follows: 0.23% C, 0.51% Si, 1.44% Mn, 0.027% P, 0.037% S, 0.23% Cr, 0.12% Ni, 0.17% Cu, 0.083% V, and Fe (balance).

The saturated calcium hydroxide solution served as the SCP solution. The pH value was approximately 12.5. The mass fraction of NaCl in the SCP solution was 1.0% or 3.5%. The concentration of sodium molybdate was 0, 0.1, 0.3, 0.5, 1.0, or 2.0 g/L. All reagents were analytically pure and were provided by Shanghai Aladdin Bio-Chem Technology Co. LTD. The distilled water was used for dissolution.

2.2 Electrochemical measurements

One end of the FGHS reinforcement served as the working surface and the other end was welded to a copper wire. All parts except the working surface were sealed with epoxy resin. The working area was 2.01 cm^2. The working surface was sequentially ground with metallographic paper in a stepwise manner from No. 200 to No. 2000, and then scrubbed with acetone, rinsed with distilled water, and dried with cold air.

The electrochemical measurements were performed on a CHI760D electrochemical workstation (CH Instruments, Inc.). Potentiodynamic polarization curves, EIS spectra, and Mott–Schottky curves were recorded. A three-electrode system, consisting of the FGHS reinforcement as the working electrode, a platinum electrode as the auxiliary electrode, and a saturated calomel electrode (SCE) as the reference electrode, was used. Prior to each electrochemical measurement, the reinforcement was exposed to the test solution for 1 h to obtain a steady open-circuit potential. All of the tests were conducted at room temperature. To ensure the reliability of the results, each test was repeated 3–5 times.

EIS measurements were performed at open-circuit potential. The frequency ranged from 100 kHz to 0.01 Hz. The amplitude of the signal was 5 mV.

The potentiodynamic polarization curves were measured from the cathodic direction, which was negatively shifted by 300 mV from the open-circuit potential, to the anodic direction until the anodic current increased rapidly. The scan rate was 1 mV/s. The polarization parameters such as corrosion current density (i_{corr}), corrosion potential (E_{corr}), the breakdown potential (E_b) were analyzed with the software attached to the test instrument.

Using the impedance–potential technique, the curve of the impedance (Z) versus the electrode potential (E) was first obtained. The interfacial capacitance (C_{sc}) was then determined based on the Z value. The C_{sc}^2–E curve, i.e., the Mott–Schottky curve, was then obtained. In accordance with Mott–Schottky theory [40, 41], the semiconductor type and carrier density of the corrosion product layer on the surface of the FGHS reinforcement were determined.

2.3 Microscopic analysis

The morphologies of the FGHS reinforcement samples corroded in the tested SCP solutions for 5 h were examined using SEM (EVO-18 model), and the corresponding chemical compositions were determined using EDS (X-MAX 20).

3. RESULTS AND DISCUSSION

3.1 Surface corrosion morphology

Figure 1 presents SEM images showing the corrosion morphology of samples of FGHS reinforcement after immersion in SCP solutions containing various concentrations of NaCl. As shown in Fig. 1(a), after immersion in the pure SCP solution, the passivation film on the surface of the FGHS reinforcement was completely continuous. EDS analysis revealed a high abundance of oxygen in the

film. That is, the passivation film consisted of iron oxides and hydroxides, as reported in the literature [42, 43].

However, in the presence of 1.0% NaCl, the corrosion surface was bubbled and cracked, leading to the destruction of the continuity of the film (Fig. 1(b)). EDS analysis revealed that the uncracked film contained a high abundance of oxygen and no chloride, whereas the cracked regions displayed a high abundance of chloride and substantially decreased oxygen content.

In the presence of 3.5% NaCl, the passivation film was severely damaged (Fig. 1(c)). Almost the entire layer was severely cracked with a clearly increased roughness. The corrosion products contained a high abundance of chloride, and the coarser and more protruding the corrosion products were, the higher the chloride content was. These results indicate that the passivation film is continuous and complete in the absence of chloride and bubbled, cracked, and less compact in the presence of chloride, weakening or even eliminating its protective effect.

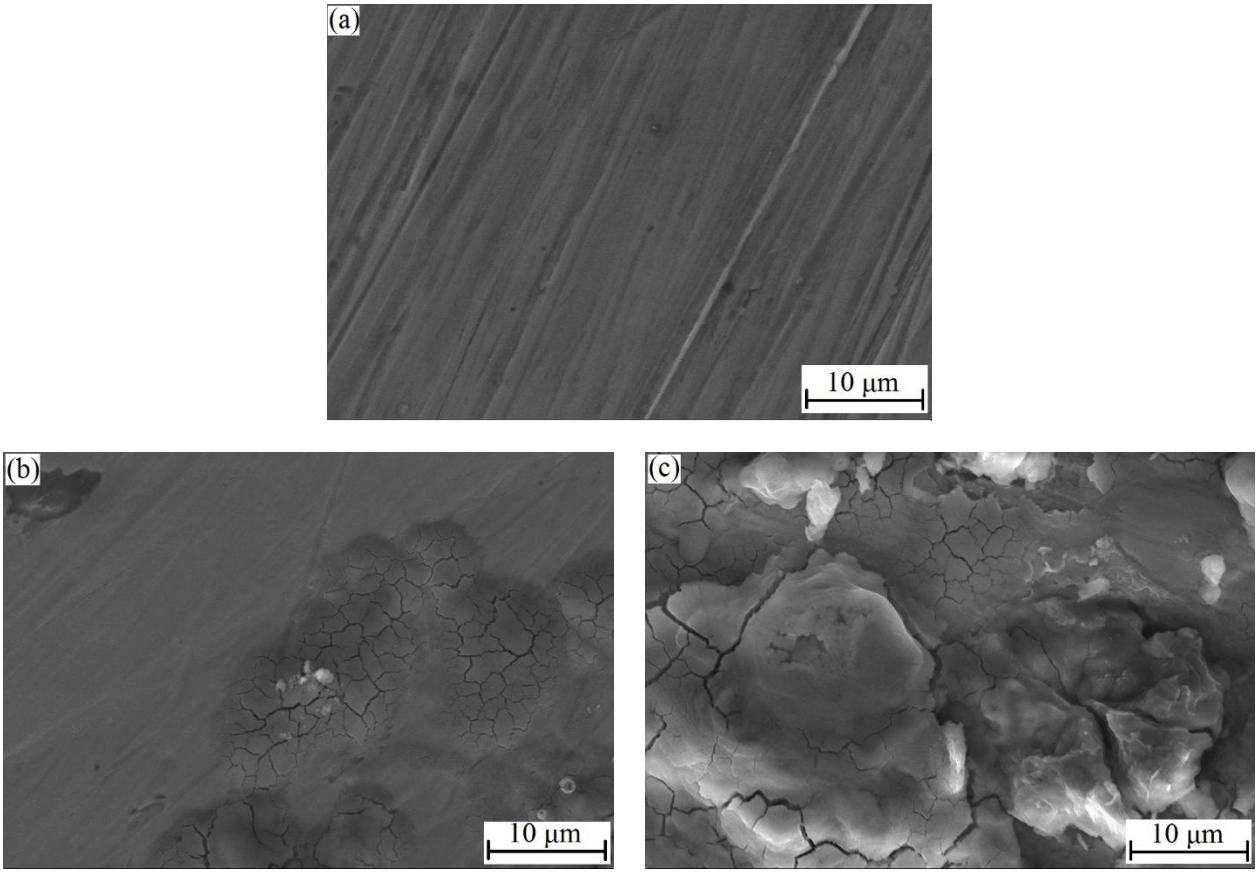

Figure 1. SEM images showing the corrosion morphology of samples of FGHS reinforcement after immersion in SCP solutions (a) without NaCl, (b) with 1.0% NaCl, and (c) with 3.5% NaCl.

Figure 2 shows the influence of molybdate on the corrosion morphology of FGHS reinforcement. Upon the addition of molybdate to the SCP solution containing 1.0% NaCl, no pits were observed on the reinforcement surface and the passivation film was almost continuous (Fig. 2(a)). When the NaCl concentration was increased to 3.5%, a few pits were observed but there were still no cracks (Fig. 2(b)). EDS analysis revealed that no chloride was present in the film. These results suggest

that molybdate inhibits the involvement of chloride ions in the film formation. Thus, molybdate acts as an inhibitor to make the passivation film more continuous and complete.

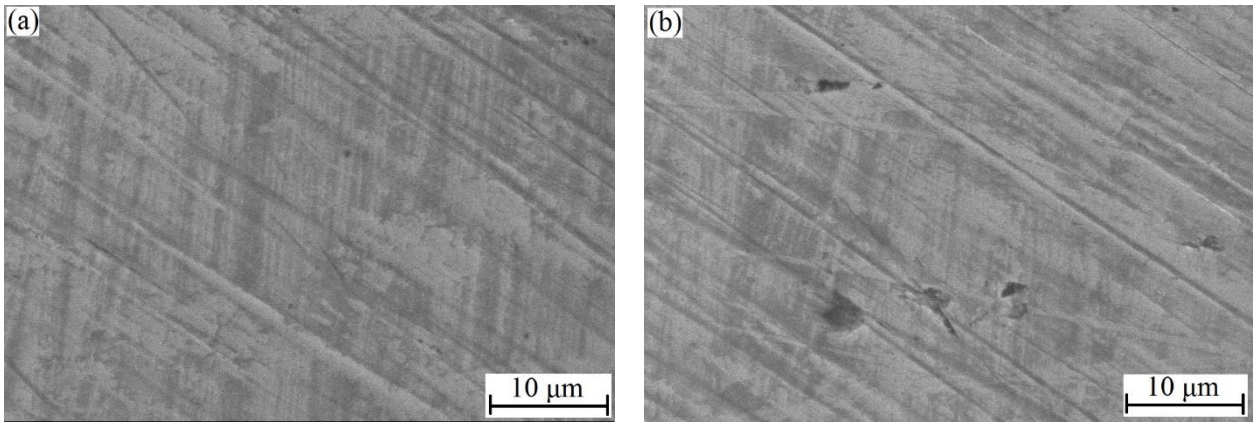

Figure 2. SEM images showing the influence of molybdate on the corrosion morphology of samples of FGHS reinforcement after immersion in SCP solutions containing (a) 1.0% and (b) 3.5% NaCl.

3.2 Potentiodynamic polarization curves

Figure 3 shows the potentiodynamic polarization curves for samples of FGHS reinforcement in SCP solutions containing various concentrations of sodium chloride and sodium molybdate. As shown in Fig. 3(a), the cathodic branch of the polarization curve shifted slightly to the left upon the addition of molybdate to the SCP solution containing 1.0% NaCl and remained almost unchanged with increasing sodium molybdate concentration. However, the anodic branch of the polarization curve moved substantially to the left and was greatly influenced by the sodium molybdate concentration. As the sodium molybdate concentration was increased to 0.5 g/L, the anodic branch of the polarization curve clearly shifted to the left and the breakdown potential (E_b) increased gradually. Upon further increasing the sodium molybdate concentration to 1.0 g/L, the anodic branch did not shift further left, although the E_b value improved greatly. Finally, upon increasing the sodium molybdate concentration to 2.0 g/L, the anodic curve shifted slightly to the right and the E_b value substantially decreased. Furthermore, in the presence of sodium molybdate, the corrosion potential (E_{corr}) of the FGHS reinforcement shifted in the positive direction. These results indicate that molybdate predominantly inhibits the anodic corrosion of FGHS reinforcement, i.e., it is an anodic corrosion inhibitor, similar to other corrosion systems [28-37].

As shown in Fig. 3(b), for SCP solution containing 3.5% NaCl, no passivation region was observed in the anodic curve, and the FGHS reinforcement was in the active state. This is in good agreement with the SEM results. When sodium molybdate was added, only the anodic curves underwent an obvious change, and E_{corr} shifted in the positive direction. The anodic curves initially markedly shifted to the left with increasing sodium molybdate concentration, followed by a slight right shift. The maximum left shift was observed when the sodium molybdate concentration was 1.0 g/L, similar to the case of SCP solution containing 1.0% NaCl. However, in the presence of 3.5% NaCl, there was still no passivation region in the anodic curves after the addition of sodium molybdate. These

results indicate that molybdate has only a limited effect on improving the corrosion resistance of FGHS reinforcement at high chloride concentrations.

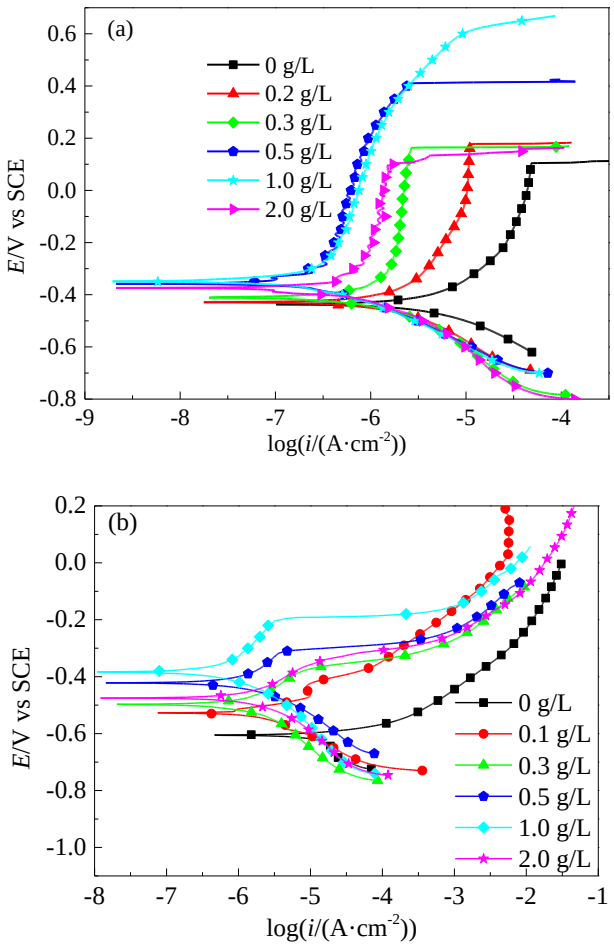

Figure 3. Effect of sodium molybdate concentration on potentiodynamic polarization curves of samples of FGHS reinforcement in SCP solutions containing (a) 1.0% and (b) 3.5% NaCl.

Upon exposing FGHS reinforcement to the alkaline SCP solution, a large number of corrosion cells are formed on the surface owing to the non-uniformity of the composition and the microstructure. Oxidation reactions of the reinforcement occur at the anode:

$$Fe \rightarrow Fe^{2+} + 2e^{-} \quad (1)$$

$$Fe^{2+} \rightarrow Fe^{3+} + e^{-} \quad (2)$$

At the cathode, the reduction of oxygen occurs under alkaline conditions:

$$O_2 + 2H_2O + 4e^{-} \rightarrow 4OH^{-} \quad (3)$$

Subsequently, a series of chemical reactions occur:

$$Fe^{2+} + 2OH^{-} \rightarrow Fe(OH)_2 \downarrow \quad (4)$$

$$Fe^{3+} + 3OH^{-} \rightarrow Fe(OH)_3 \downarrow \quad (5)$$

$$Fe(OH)_2 \rightarrow FeO + H_2O \quad (6)$$

$$2Fe(OH)_3 \rightarrow Fe_2O_3 + 3H_2O \quad (7)$$

Moreover, a portion of the FeO will be further oxidized by oxygen:

$$6FeO + O_2 \rightarrow 2Fe_3O_4 \quad (8)$$

The above reaction products, i.e., $Fe(OH)_2$, $Fe(OH)_3$, FeO, Fe_2O_3, and Fe_3O_4, are the main components of the passivation film on the surface of reinforcement in concrete media [42, 43].

In the presence of chloride ions, the competitive adsorption of hydroxyl ions and active chloride ions occurs on the reinforcement surface. As the adsorption ability of chloride ions is greater than that of hydroxyl ions, the reactions shown in Eqs. (4)–(8) are inhibited, and the loose and discontinuous compounds, which contain chloride and do not provide corrosion protection, are formed instead. Thus, the corrosion resistance of the reinforcement decreases substantially [44, 45].

In the presence of sodium molybdate, the molybdate ions play two main roles. On the one hand, the weak oxidizing ability of molybdate ions further promotes the oxidation of Fe^{2+} to Fe^{3+}, i.e., Eq. (2), with the concomitant reduction of the molybdate ions to MoO_2.

The Fe^{3+} compounds in the passivation film are denser, while the Fe^{2+} compounds are relatively looser [39, 42, 46]. Therefore, a higher Fe^{3+} content in the passivation film results in a greater density and superior corrosion resistance. Moreover, the density and corrosion resistance of the molybdenum compounds in the reduced (i.e., low-valence) state are superior to those in a high-valence (i.e., hexavalent) state [29, 34, 47]. Therefore, the addition of molybdate leads to the formation of Fe^{3+} compounds and Mo^{4+} compounds in the passivation film, which are also deposited in and repair the pits in the reinforcement [32, 38, 39]. This improves the compactness and continuity of the passivation film, and therefore also the corrosion resistance of the reinforcement.

On the other hand, molybdate ions exhibit strong adsorption and preferentially adsorb onto the defects or active points on metal surfaces [32, 33, 38]. That is, competitive adsorption of molybdate ions and chloride ions occurs at the defects of the corrosion products, thus reducing the destruction of the passivation film by the chloride ions.

At a low molybdate concentration, oxidation and adsorption are limited, and so the improvement of the corrosion resistance of the FGHS reinforcement is finite, as shown in Fig. 3. To establish a complete, effective, and compact protective film, a suitable molybdate concentration is required. However, if the molybdate concentration is too high, the oxidation capacity is further enhanced. The theoretical cathodic polarization curve moves upward and to the right, and the intersection of the theoretical cathodic and anodic curves is in the transpassivation region. The current density at the reinforcement increases and new anodic reactions emerge. Hydroxyl ions undergo oxidation to oxygen and low-valence molybdenum oxide is oxidized to a higher-valence oxide:

$$4OH^- \rightarrow O_2 + 2H_2O + 4e^- \quad (9)$$

$$MoO_2 + H_2O \rightarrow MoO_3 + 2H^+ + 2e^- \quad (10)$$

Here, the liberation of oxygen gas leads to a reduction in the compactness of the passivation film and its binding force to the matrix. The formation of the high-valence molybdenum oxide also causes a decrease in the compactness of the passivation film. The corrosion resistance of the FGHS reinforcement therefore declines.

When the concentration of chloride ions in the SCP solution is high, a large amount of chloride ions adsorb on the reinforcement surface. The protection efficiency of molybdate is not sufficient to prevent the severe destruction due to the chloride ions. Consequently, in the presence of 3.5% NaCl, passivation cannot occur and some corrosion pits are still formed on the surface of the FGHS reinforcement (Figs. 2(b) and 3(b)). The corrosion inhibition by molybdate is limited.

Figure 4 shows the influence of the sodium molybdate concentration on the corrosion current density (i_{corr}) and breakdown potential (E_b) of FGHS reinforcement in SCP solution, and Figure 5 shows the influence of the sodium molybdate concentration on the corrosion protection efficiency (P_e). Here, P_e was defined as

$$P_e(\%) = (1 - i_{corr} / i_{corr}^0) \times 100\% \quad (11)$$

Where i_{corr} and i_{corr}^0 are the corrosion current density for the FGHS reinforcement in SCP solution with and without sodium molybdate, respectively. It should be pointed out that as no passivation layer is formed on the FGHS reinforcement in SCP solution containing 3.5% NaCl, the E_b value in this case cannot be determined.

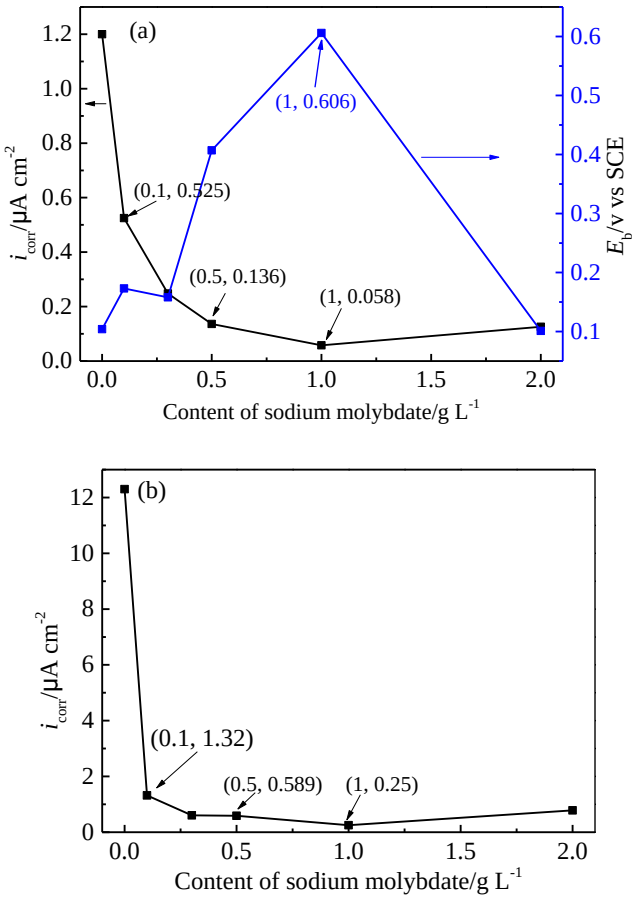

Figure 4. Influence of sodium molybdate concentration on i_{corr} and E_b of samples of FGHS reinforcement in SCP solutions containing (a) 1.0% and (b) 3.5% NaCl.

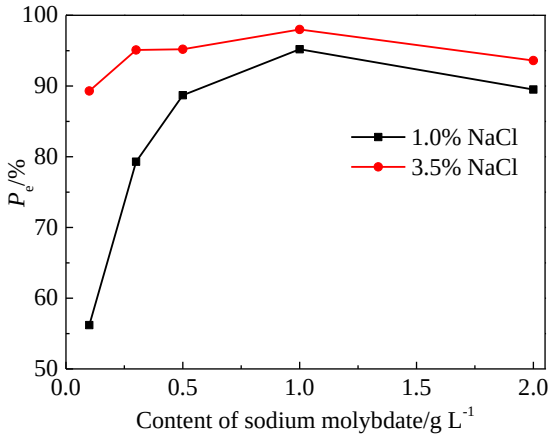

Figure 5. Influence of sodium molybdate concentration on P_e of samples of FGHS reinforcement in SCP solutions containing 1.0% and 3.5% NaCl.

As shown in Fig. 4, with increasing sodium molybdate concentration, the i_{corr} of the FGHS reinforcement initially decreased rapidly and then decreased more slowly, followed by a slight increase, in both of the SCP solutions. The opposite trend was therefore observed for P_e, as shown in Fig. 5. The optimum concentration of sodium molybdate was 1.0 g/L in both cases. In SCP solution containing 1.0% NaCl, the E_b of the reinforcement first increased and then decreased, with the maximum at 0.606 V versus SCE, which is equivalent to that in pure SCP solution. This indicates that under these conditions the passivation film on the FGHS reinforcement possessed sufficient density and continuity. This is also clearly demonstrated by the SEM images shown in Figs. 1 and 2.

The polarization parameters of the FGHS reinforcement in the SCP solutions containing 1.0% NaCl and 3.5% NaCl were also compared. The i_{corr} value of the former (0.058 μA·cm^{-2}) was considerably smaller than that of the latter (0.250 μA·cm^{-2}). The E_{corr} value of the former was also clearly greater than that of the latter. The corrosion electrochemical indices of the former were superior to those of the latter. This could mainly be attributed to the reduced corrosion by the lower concentration of chloride ions and the good inhibition of corrosion by molybdate. However, the P_e values were noticeably smaller in the presence of 1.0% NaCl than in the presence of 3.5% NaCl under the same conditions, as shown in Fig. 5; the maximum values of P_e were 95.2% and 98.0%, respectively, because the i_{corr} value of the latter was considerably greater than that of the former. This is similar to the corrosion inhibition of FGHS and plain reinforcement by nitrate [16, 48]. Therefore, in addition to P_e, other indices such as i_{corr} and E_b should also be considered to comprehensively evaluate the performance of inhibitors of metal corrosion.

3.3 EIS diagrams

Figures 6 and 7 show the influence of the sodium molybdate concentration on the EIS diagrams for samples of FGHS reinforcement in SCP solutions containing 1.0% NaCl and 3.5% NaCl, respectively. As shown in Figs. 6a and 7a, irrespective of whether sodium molybdate was present in the SCP solution, the Nyquist diagrams revealed two time constants, i.e., a high-frequency capacitance arc and a low-frequency capacitance arc. These can also be observed in Figs. 6b and 7b, where the

frequency of the peaks of the negative phase angle is high and wide. The high-frequency capacitance arc corresponds to the corrosion product film, and the low-frequency capacitance arc is associated with the double-layer capacitance of the interface between the reinforcement and solution [49, 50]. Moreover, the capacitance arcs in the Nyquist diagrams of all samples were deformed. The center of the semicircular arc was in the fourth quadrant, and the peak value of the negative phase angle was less than 90°. These phenomena indicate that both the capacitance of the corrosion product film and the double-layer capacitance of the reinforcement/solution interface exhibit dispersion effects. These effects can be ascribed to the heterogeneity of the thickness and density of the corrosion product film on the FGHS reinforcement surface [49-51].

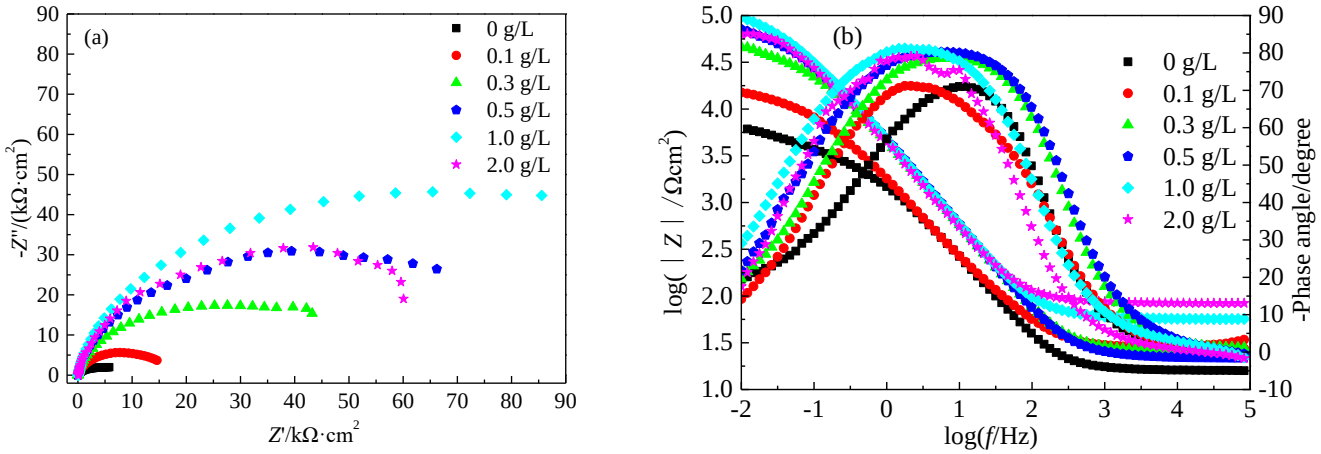

Figure 6. Influence of sodium molybdate concentration on the (a) Nyquist and (b) Bode diagrams of samples of FGHS reinforcement in SCP solutions containing 1.0% NaCl.

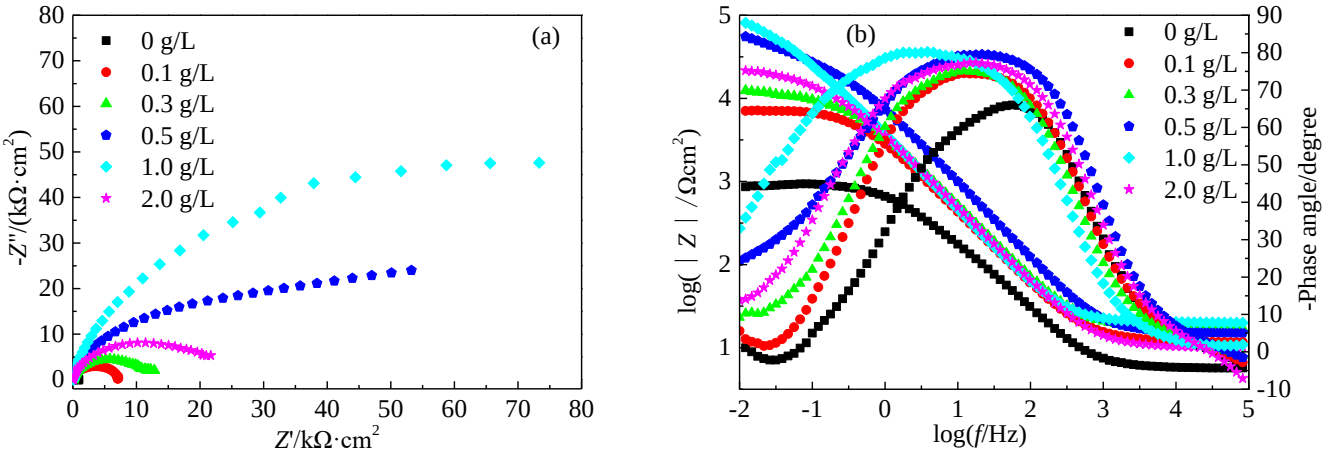

Figure 7. Influence of sodium molybdate concentration on the (a) Nyquist and (b) Bode diagrams of samples of FGHS reinforcement in SCP solutions containing 3.5% NaCl.

In general, a larger capacitance arc indicates a higher impedance of the metal, and therefore a more difficult corrosion reaction. The impedance at low frequency is higher, and the peak value of the negative phase angle is larger and closer to the low-frequency end. Therefore, this indicates improved

corrosion resistance [49]. A smaller dispersion of the capacitance arc can be considered to indicate a larger thickness and greater compactness of the layer on the metal surface.

As shown in Figs. 6 and 7, in the presence of molybdate, the size of the capacitance arc and the impedance at the low-frequency end increased for both SCP solutions. The peak value of the negative phase angle was also enhanced and shifted toward the low-frequency region. Furthermore, upon increasing the sodium molybdate concentration from 0 g/L to 2.0 g/L, the size of the capacitance arc, the impedance at the low-frequency end, and the peak value of the negative phase angle first increased and then slowly decreased. The optimum sodium molybdate concentration was 1.0 g/L. However, the EIS parameters of the FGHS reinforcement in SCP solutions containing 1.0% NaCl were larger than those in SCP solutions containing 3.5% NaCl at the same sodium molybdate concentration. It can also be considered that molybdate afforded better corrosion inhibition for FGHS reinforcement in SCP solution containing a lower concentration of chloride ions. These findings are in good agreement with the results from the polarization curves and corrosion morphology analysis.

3.4 Mott–Schottky curves

In general, passivation films or oxide films on metal surfaces possess semiconductor properties. When in contact with the solution, the semiconductor film has the opposite charge to the solution. The excess charges are distributed in the space charge layer. When the space charge layer is depleted, the relationship between the space charge capacitance (C_{sc}) and the electrode potential (E) can be analyzed using the Mott–Schottky equations [40, 41]:

$$n\text{-type: } \frac{1}{C_{sc}^2} = \frac{2}{\varepsilon_0 \varepsilon e N_D}\left[E - E_{fb} - \frac{kT}{e}\right] \tag{12}$$

$$p\text{-type: } \frac{1}{C_{sc}^2} = -\frac{2}{\varepsilon_0 \varepsilon e N_A}\left[E - E_{fb} - \frac{kT}{e}\right] \tag{13}$$

where ε_0 is the dielectric constant of a vacuum (8.854×10^{-12} F/m), ε is the relative dielectric constant of the passivation film (approximately 12) [46], e is the elementary charge (1.602×10^{-19} C), N_D and N_A are the donor density and acceptor density of *n*-type and *p*-type semiconductors, respectively, E_{fb} is the flat-band potential, k is the Boltzmann constant (1.38×10^{-23} J/K), and T is the thermodynamic temperature. At room temperature, kT/e is approximately 25 mV and can be neglected. When the slope of the curve is positive, the passivation film is an *n*-type semiconductor. When the slope of the curve is negative, the passivation film is a *p*-type semiconductor. N_D and N_A can be obtained based on the slope, and E_{fb} can be obtained according to the slope and intercept.

Figure 8 presents the Mott–Schottky curves for samples of FGHS reinforcement in SCP solutions containing 1.0% or 3.5% NaCl. In the presence of 1.0% NaCl, all of the Mott–Schottky curves changed continuously and included two linear segments with positive slopes. Thus, the corresponding passivation films were *n*-type semiconductors. These consisted of two types of carriers, i.e., shallow donors of oxygen vacancies and Fe^{2+}, and deep donors of oxygen vacancies and Fe^{3+}. This coincides with the results obtained for the corrosion inhibitors of nitrate, phosphate, and dioctyl sebacate for HSFG reinforcement [16-18]. A higher content of Fe^{3+} leads to a lower content of oxygen vacancies, a smaller N_D value, and thus superior corrosion protection by the corrosion product film. On

the contrary, a lower content of Fe^{3+} leads to a worse anticorrosion performance of the corrosion product [42, 46, 52]. Upon increasing the sodium molybdate concentration from 0 g/L to 2.0 g/L, the slope first increased and then slightly decreased, and the curves first moved up and then slightly down. When the sodium molybdate concentration was 1.0 g/L, the maximum slope and highest curve were obtained.

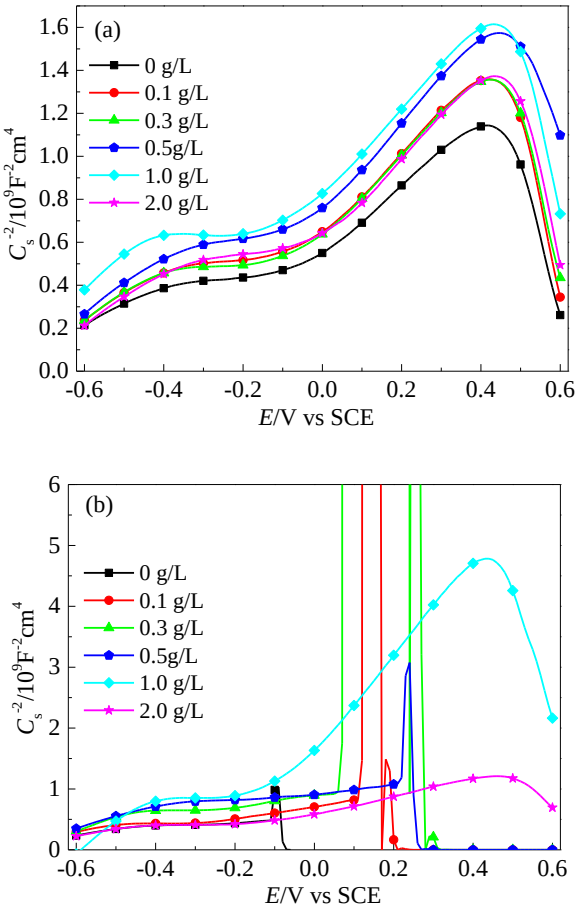

Figure 8. Mott–Schottky curves for samples of FGHS reinforcement in SCP solutions containing various concentrations of sodium molybdate and (a) 1.0% or (b) 3.5% NaCl.

In the presence of 3.5% NaCl, all of the Mott–Schottky curves except those for 1.0 g/L and 2.0 g/L sodium molybdate were discontinuous at higher *E* values. The participation of chloride ions in the formation of the film led to decreased compactness and continuity of the corrosion product layer. The adsorption of a large amount of chloride ions on the reinforcement resulted in inhibition of the adsorption of molybdate ions. The concentrations of Fe^{3+} and MoO_2 were thus decreased, whereas the concentration of oxygen holes was conversely increased. At higher values of *E*, the supply of Fe^{3+} was exhausted and the semiconductor characteristics were not observed. Furthermore, with increasing molybdate concentration, the value of *E* where the discontinuous changes occur was increased. This indicates increased concentrations of Fe^{3+} and MoO_2, a decreased concentration of oxygen holes, and a relatively improved corrosion resistance by the corrosion product layer.

Tables 1 and 2 summarize the semiconductor characteristics. Upon the addition of molybdate to the SCP solutions, the values of $N_{D,1}$ and $N_{D,2}$ decreased and the values of $E_{fb,1}$ and $E_{fb,2}$ shifted toward the positive direction. With increasing sodium molybdate concentration, both $N_{D,1}$ and $N_{D,2}$ first clearly increased and then decreased slightly. The minimum values were observed for a sodium molybdate concentration of 1.0 g/L. These are in good agreement with the experimental results described above.

Table 1. Influence of sodium molybdate concentration on semiconductor characteristics of the corrosion products on FGHS reinforcement in SCP solution containing 1.0% NaCl.

Sodium molybdate concentration/ g L^{-1}	−0.6 to −0.3 V vs SCE		−0.1 to 0.4 V vs SCE	
	$N_{D,1}$/(×10^{20} cm^3)	$E_{fb,1}$/V vs SCE	$N_{D,2}$/(×10^{19} cm^3)	$E_{fb,2}$/V vs SCE
0	1.707	−0.960	7.050	−0.355
0.1	1.136	−0.836	6.119	−0.309
0.3	1.050	−0.839	5.116	−0.308
0.5	0.991	−0.822	5.093	−0.304
1.0	0.781	−0.785	4.625	−0.294
2.0	1.042	−0.808	5.194	−0.328

Table 2. Influence of sodium molybdate concentration on semiconductor characteristics of the corrosion products on FGHS reinforcement in SCP solution containing 3.5% NaCl.

Sodium molybdate concentration/ g L^{-1}	−0.6 to −0.3 V vs SCE		−0.1 to 0.4 V vs SCE	
	$N_{D,1}$/(×10^{20} cm^3)	$E_{fb,1}$/V vs SCE	$N_{D,2}$/(×10^{19} cm^3)	$E_{fb,2}$/V vs SCE
0	2.034	−0.980	Discontinuous changes	
0.1	1.094	−0.871		
0.3	1.089	−0.816		
0.5	1.017	−0.782		
1.0	0.697	−0.813	2.520	2.520
2.0	0.723	−0.823	11.662	11.662

4. CONCLUSIONS

The corrosion inhibition performance of sodium molybdate was investigated for samples of FGHS reinforcement immersed in SCP solutions containing 1.0% or 3.5% NaCl.

Sodium molybdate was a good corrosion inhibitor for FGHS reinforcement in both SCP solutions. Upon increasing the sodium molybdate concentration from 0 g/L to 2.0 g/L, the corrosion current density (i_{corr}) of the reinforcement and the donor density (N_D) in the corrosion product layer first clearly decreased and then slightly increased. The optimum sodium molybdate concentration was 1.0 g/L. A lack of molybdate led to poor corrosion inhibition, whereas excessive molybdate both reduced the corrosion resistance and is a waste of resources.

The corrosion protection efficiency (P_e) of molybdate for FGHS reinforcement in SCP solution containing 1.0% NaCl was inferior to that in SCP solution containing 3.5% NaCl. However, the i_{corr} of

the former (0.058 μA cm^{-2}) was considerably lower than that of the latter (0.250 μA cm^{-2}). The Mott–Schottky curves for the former were continuous, whereas some of those for the latter were not. Almost no corrosion pits in the FGHS reinforcement were observed for the former, whereas a few pits were still observed for the latter. Molybdate exhibits good corrosion inhibition for FGHS reinforcement at low concentrations of chloride ions, although other corrosion inhibitors or composite inhibitors should be considered for high chloride ion concentrations.

During the evaluation of inhibitors of metal corrosion, other electrochemical indices such as i_{corr}, E_b, and impedance should also be considered in addition to P_e.

ACKNOWLEDGMENTS

This work was financially supported by the National Natural Science Foundation of China (Nos. 51578255 and 51778247), the Natural Science Foundation of Fujian Province (No. 2017J01489), and Program for Innovative Research Team in Science and Technology in Fujian Province University.

References

1. A. B. Araz, F. Li, R. T. Patricia, D. Ponge and D. Raabe, *Mater. Sci. Eng., A*, 463 (2006) 138.
2. J. X. Fu, T. Li, E. Y. Zhu and C. J. Wu, *Appl. Mech. Mater.*, 654 (2014) 35.
3. Y. F. Mi, *Process study of VN microalloyed 500MPa seismic steel bar*, Kunming University of Science and Technology, 2011, Kunming, China.
4. Q. X. Dai, *Metal Material Science*, Chemical Industry Press, 2011, Beijing, China.
5. R. Manoharan, P. Jayabalan and K. Palanisamy, "Experimental study on corrosion resistance of TMT bar in concrete,"International Conference on Construction and Building Technology, 2008, pp. 239, India.
6. S. K. Paul, P. K. Rana, D. Das, S. Chandra and S. Kundu, *Constr. Build. Mater.*, 54 (2014) 170.
7. D. W. Li, *Experimental research of anchorage properties for fine-grained steel bars in concrete*, Zhengzhou University, 2010, Zhengzhou, China.
8. Q. F. Wang, H. C. Wu, Y. Y. Xu, Y. X. Yang and Z. Y. Huo, *J. Build. Struct.*, 32 (2011) 120.
9. M. B. Yu, *Study on shear capacity of reinforced concrete beam with 500 MPa hot rolled bars of fine grains*, Huaqiao University, 2011, Xiamen, China.
10. S. B. Lyon, in *Corrosion of Carbon and Low Alloy Steels, Shreir's Corrosion*, 3rd., B. Cottis, M. Graham, R. Lindsay, S. Lyon, T. Richardson, D. Scantlebury, and H. Stott, Editor, p.1693, Elsevier Science, Amsterdam (2010)
11. M. A. Islam, *Procedia Eng.*, 125 (2015) 623.
12. J. J. Shi, W. Sun and G. Q. Geng, *Acta Metall. Sin.*, 47 (2011) 449.
13. J. J. Shi, W. Sun, G. Q. Geng and J. Y. Jiang, *J. Univ. Sci. Technol. B.*, 33 (2011) 1471.
14. H. T. Sarraf and A. Poursaee, *Constr. Build. Mater.*, 167 (2018) 680.
15. B. L. Lin and Y. Y. Xu, *J. Zhenzhou Univ. Light Ind. (Natural Sci.)*, 25 (2010) 45.
16. B. L. Lin and Y. Y. Xu, *Int. J. Electrochem. Sci.*, 11 (2016) 3824.
17. B. L. Lin, C. N. Liu, Z. Luo, J. D. Li, S. Wang and Y. Y. Xu, *Int. J. Electrochem. Sci.*, 12 (2017) 2070.
18. B. L. Lin, Z. Luo, C. N. Liu, X. F. Liu and Y. Y. Xu, *Int. J. Electrochem. Sci.*, 12 (2017) 8892.
19. B. L. Lin and Y. Y. Xu, *J. Build. Mater.*, 19 (2016) 1082.
20. T. U. Mohammed, N. Otsuki and M. Hisada, *J. Mater. Civ. Eng.*, 13 (2001) 194.
21. T. U. Mohammed, N. Otsuki and M. Hisada, *Cem. Concr. Res.*, 31 (2001) 829.
22. M. P. Papadopoulos, C. A. Apostolopoulos and N. D. Alexopoulos, *Mater. Des.*, 28 (2007) 2318.
23. J. H. Jiang, Y. S. Yuan, F. M. Li, B. Wang and Y. S. Ji, *J. Build. Mater.*, 12 (2009) 523.

24. O. Geng, Y. S. Yuan, F. M. Li, Q. Wu and J. D. Zhang, *J. China Univ. Min. Technol.*, 35 (2006) 488.
25. W. Z. Gan, W. L. Jin and T. N. Xu, *J. Build. Mater.*, 12 (2009) 699.
26. G. Li, N. Otsuki and Y. S. Yuan, *J. China Univ. Min. Technol.*, 38 (2009) 149.
27. L. Wang, Y. Ma, W. Ding, J. Zhang and Y. Liu, *J. Perform. Constr. Facil.*, 29 (2015) 04014163.
28. X. L. Guo, Z. C. Feng, B. Hurley and R. Buchheit, *J. Electrochem. Soc.*, 163, (2016) C260.
29. M. A. Jakab, F. Presuel-Moreno and J. R. Scully, *J. Electrochem. Soc.*, 153, B244 (2006).
30. W. D. Robertson, *J. Electrochem. Soc.*, 98 (1951) 94.
31. S. A. M. Refaey, S. S. Abd El-Rehim, F. Taha, M. B. Saleh and R. A. Ahmed, *Appl. Surf. Sci.*, 158 (2000) 190.
32. C. B. Zheng, L. Cai, Z. J. Tang and X. L. Shen, *Surf. Coat. Technol.*, 287 (2016) 153.
33. Y. Zhou, Y. Zuo and B. Lin, *Mater. Chem. Phys.*, 192 (2017) 86.
34. Y. Zhou and Y. Zuo, *Appl. Surf. Sci.*, 353 (2015) 924.
35. Y. T. Tan, S. L. Wijesinghe and D. J. Blackwoodc, *J. Electrochem. Soc*., 164 (2017) C505.
36. Y. T. Tan, S. L. Wijesinghe and D. J. Blackwood, *J. Electrochem. Soc.*, 163 (2016) C649.
37. Y. M. Tang, G. D. Zhang and Y. Zuo, *Constr. Build. Mater.*, 28 (2012) 327.
38. H. Verbruggen, H. Terryn and I. D. Graeve, *Constr. Build. Mater.*, 124 (2016) 887.
39. X. Zhou, H. Y. Yang and F. H. Wang, *Corros. Sci. Prot. Technol.*, 22 (2010) 343.
40. A. Fattah-alhosseini and S. Vafaeian, *J. Alloys Compd.*, 639 (2015) 301.
41. I. M. Gadala and A. Alfantazi, *Appl. Surf. Sci.*, 357 (2015) 356.
42. W. Chen, R. G. Du, R. G. Hu, H. Y. Shi, Y. F. Zhu and C. J. Lin, *Acta Metall. Sin.*, 47 (2011) 735.
43. Y. Peng, L. Liu, S. L. Wang, Y. H. Lin, Y. R. Sun and R. C. Xia, *J. Pet. Sci. Eng.*, 167 (2018) 949.
44. R. François, S. Laurens and F. Deby, "Steel corrosion in reinforced concrete," in *Corrosion and its Consequences for Reinforced Concrete Structures*, pp. 1 (2018).
45. L. H. Jiang, G. H. Huang, J. X. Xu, Y. R. Zhu and L. L. Mo, *Constr. Build. Mater.*, 30 (2012) 516.
46. J. Luo, Y. Wang, J. B. Jiang, Q. D. Zhong, Z. Y. Zhu and L. Zhang, *Acta Chim. Sin.*, 70 (2012) 1213.
47. X. J. Gong, Y. C. Li, K. R. Peng and X. J. Xie, *Corros. Sci. Prot. Technol.*, 13 (2001) 208.
48. B. Qiao, R. G. Du, W. Chen, Y. F. Zhu and C. J. Lin, *Acta Metall. Sin.*, 46 (2010) 245.
49. C. N. Cao and J. Q. Zhang, *An Introduction to Electrochemical Impedance Spectroscopy*, Science Press, 2004, Beijing, China.
50. D.V. Ribeiro and J. C. C. Abrantes, *Constr. Build. Mater.*, 111 (2016) 98.
51. A. Benedetti, P. Sumodjo and K. Nobe, *Electrochim. Acta*, 40 (1995) 2657.
52. J. S. Kim, E. A. Cho and H. S. Kwon, *Corros. Sci.*, 43 (2001) 1403.